Available online at www.sciencedirect.com
ScienceDirect
PHOTONICS AND NANOSTRUCTURES Fundamentals and Applications
Photonics and Nanostructures – Fundamentals and Applications 7 (2009) 170–175
www.elsevier.com/locate/photonics

Metal grating on a substrate nanostructure for sensor applications

A. Karabchevsky [a], O. Krasnykov [a], I. Abdulhalim [a], B. Hadad [b], A. Goldner [b], M. Auslender [c,*], S. Hava [c]

[a] Department of Electro-Optics Engineering, Ben-Gurion University of the Negev, POB 653, Beer Sheba 84105, Israel
[b] The Weiss Family Laboratory for Nanoscale Systems, Ben-Gurion University of the Negev, POB 653, Beer Sheba 84105, Israel
[c] Department of Electrical and Computer Engineering, Ben-Gurion University of the Negev, POB 653, Beer Sheba 84105, Israel

Received 2 February 2009; received in revised form 29 April 2009; accepted 7 May 2009
Available online 13 May 2009

Abstract

Extraordinary optical transmission via periodic array of sub-wavelength slits in a metal layer on a dielectric substrate is revisited for sensing applications. Numerical case studies using an in-house software tool showed two peaks of enhanced transmission, one being very sensitive to the ambient index and another to the substrate index. Based on this, we designed and realized an optical sensor with sensitivity of the order of 400 nm/RIU.

PACS : 42.25.Bs; 42.25.Fx; 42.79.Dj

Keywords: Extraordinary optical transmission; Diffraction gratings; Optical sensors

1. Introduction

The field of chemical and biological optical sensors is vastly developing, due to the needs for highly sensitive, rapid, specific and reliable, environmental control and medical diagnostics. First optical sensors of the CO_2 and O_2 gases concentration were developed [1] based on detecting changes in the absorption spectra. In the early 80s surface plasmon resonance (SPR) phenomenon was first shown [2] to be practical for both chemical and biological sensing. Since then, the SPR-based sensors have been receiving continuously growing attention [3]. In spite of highest sensitivity achieved in the sensors exploiting SPR [4], other phenomena are extensively discussed as candidates for use in a new generation of optical sensors. The phenomenon of extraordinary (or enhanced) optical transmission (EOT) reported a decade ago [5], is an unusual effect when transmittance of light through sub-wavelength apertures in a metal layer exceeds the geometric limit, i.e. the relative aperture area ratio. Recently, EOT via two-dimensional (2D) structure similar to that in [5] was shown to be capable of detecting biological molecules bound to the surface [6]. As it is known these days [7–12], one-dimensional (1D) grating, i.e. periodic array of slits, in a metal film can also support EOT. Hence it is timely to inquire possible use of the EOT enabled metallic gratings for sensing, especially because the established nano-technology allows one to fabricate the 1D gratings with much more controllable structural dimensions and easier than the 2D ones. Very recently [13], sensitivities to the refractive index (RI) changes in an analyzed substance (analyte) using periodic arrays of holes (600 nm period) in gold were compared with that of slits showing a better sensitivity for the later.

* Corresponding author. Tel.: +972 8 6461583; fax: +972 8 6472949.
E-mail address: marka@ee.bgu.ac.il (M. Auslender).

1569-4410/$ – see front matter
doi:10.1016/j.photonics.2009.05.001

The purpose of the present work is further development of the metallic EOT grating for sensor applications. The nanostructures were designed, fabricated and then used for sensing in water. The ability of the sensor is evaluated by testing the pure and ethanol contaminated de-ionized water (DIW), and the sensitivity (S) and detection limit (DL) are estimated. The EOT studies reported so far deal with the patterned Ag and Au layers. Smooth Ag and Au layers are used in common SPR sensors [2–4] (however the Au layer only protects the Ag surface). Besides, the Au surfaces easily affix cells receptors, which is functional for the biosensors. To fabricate the gratings we also used Ag and Au (on a SiO_2 substrate). The uncoated gratings, and Ag gratings coated with Au and poly-methyl-methacrylate (PMMA) were explored.

2. Optical sensors: general schematics and figures of merit

The sensors, we focus on, are systems which comprise light input/output (I/O) setups and optical components that employ strong optical effects for sensing. The analyte contacts the sensing unit, so that physical, chemical or biological changes in the former cause the changes in optical response of the latter. The readout may use the transmission or reflection modes, with the wavelength (λ) or the incidence angle (θ) scans being performed in each mode. When the effect employed is resonance like, i.e. the scanned optical response has pronounced peak or dip at $\lambda = \lambda_m$ or $\theta = \theta_m$, and the above changes in the analyte can be expressed by variation in its RI Δn_a, the sensitivity S and the detection limit DL are defined as follows:

$$S_\lambda = \frac{\Delta\lambda_m}{\Delta n_a}, \quad S_\theta = \frac{\Delta\theta_m}{\Delta n_a}; \quad \mathrm{DL}_\lambda = \frac{\delta\lambda}{S_\lambda}, \quad \mathrm{DL}_\theta = \frac{\delta\theta}{S_\theta}. \quad (1)$$

Here $\Delta\lambda_m$ and $\Delta\theta_m$ are the peak/dip shifts associated with Δn_a, $\delta\lambda$ and $\delta\theta$ are the minimal λ- and θ-scan resolutions, respectively. The definition of S and DL, when the non-resonant and near-field effects (to sense highly inhomogeneous biological analytes) are employed, is outside the scope of our study. For the two types of scan, DL has the same measure of RI units (RIU), so the smaller the DL is the more sensitive the sensor. In the present work we concentrate on the λ-scan.

3. Transmission via metallic gratings: regularities and design considerations

The metallic gratings which exhibit EOT are fairly different with regard to the dimensions and ambient materials although their typical attribute is slits of a sub-wavelength width $W < \lambda$, and a small aperture $W/\Lambda \ll 1$, where Λ is the grating period. As far as the spectral range is concerned, the EOT bands may appear both in the multi- and zero-order diffraction regimes, when $\lambda < \Lambda$ and $\lambda \geq \Lambda$, respectively [5,7–12].[1] It was recognized after Porto et al. [7] that the EM analysis including only one Bloch mode supported by the slit array, which has no cut-off in TM polarization, is sufficient to explain the EOT regularities. This single-mode approximation elaborated further in [9–11], leads to an EOT scenario at $\lambda \geq \Lambda$ as an interplay of two effects. One is launching grating-coupled SP like modes on the grating interfaces, at $\lambda \sim \lambda_{SP} \sim \Lambda$ (the SP wavelength) and the other is exciting cavity-resonance like modes inside the slit, at λ well above Λ, possible if the ratio H/λ is not too small, where H is the grating thickness [9,11].

Using the above SP like modes seems attractive for the sensors where the analyte touches the grating top or bottom, as the associated EOT peaks depend strongly on the top ambient and substrate RI [7,9]. Moreover, fabricating the gratings with as high H/λ ratios as required [7,9,11] for realizing the cavity resonances, may prove faulty. Therefore, we designed the gratings with Λ from 400 to 600 nm to be etched in Ag and Au layers with H in the range 40–100 nm deposited on a 300 μm silica substrate. To protect the Ag lines, we tried a 5 nm Au coating and a PMMA coating. We have observed (not presented here) that the Au layer corrodes in a short time, whereas thicker coatings cause the transmittance (T) and S_λ to drop significantly. Hence, we looked for a coating which would provide the sensor's stability without deteriorating T and S_λ, and found the colorless highly transparent polymer PMMA to have high potential for our design. Prefabrication simulations of the T spectra are advantageous for a smart design. To this end, due to failure of the above single-mode approximation [7,9] at such small H/λ (about 0.1–0.2) [11] that we have, we used rigorous coupled wave analysis (RCWA). We compute the diffraction-efficiency spectra of the grating nanostructures using an in-house graphically interfaced interactive toolbox [14], which implements a homebrewed code of RCWA enhanced to achieve absolute numerical stability and efficient convergence [14,15].

Fig. 1 shows the zero-order T spectra simulated for Ag gratings with the dimensions: $\Lambda = 600$ nm, $W = 36$ nm and $H = 50$ nm in different ambient. For

[1] We have no room to overview EOT as such, so our citation is far from being complete in any sense.

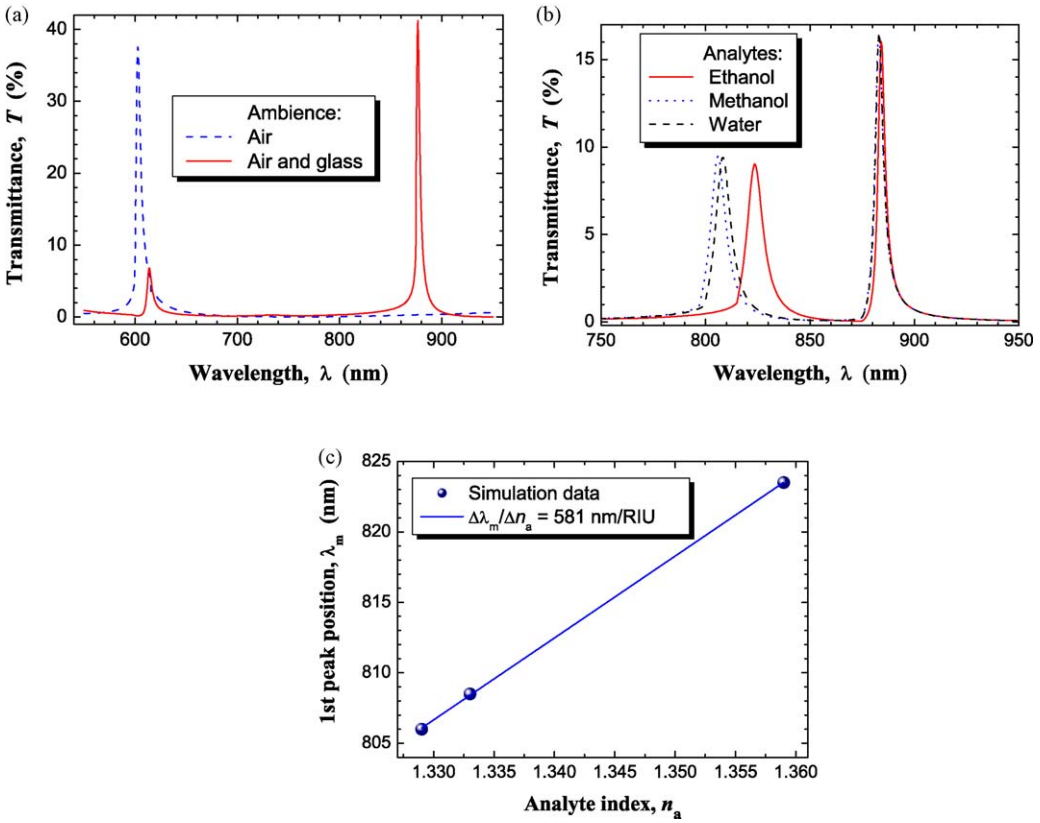

Fig. 1. The transmission spectra of the Ag grating with the dimensions: $\Lambda = 600$ nm, $W = 36$ nm and $H = 50$ nm, obtained at prefabrication stage: (a) bare grating in air (dashed line), the grating on silica substrate in air (solid line); (b) the grating on the substrate, topped by water (dashed line), methanol (dotted line) and ethanol (solid line); (c) the 1st EOT peak position vs. the analyte RI, S_λ is determined from the linear regression according to Eq. (1).

air ambient, the spectrum displays one EOT peak due to a degeneracy of the top and bottom SP like modes [7,9–12]. The degeneracy is removed if the ambient and substrate RI, e.g. n_a and n_s, respectively, become different. Then, as shown in Fig. 1(a) for $n_a = 1.000$ (air) and $n_s = 1.458$ (SiO_2), the additional EOT peak splits off the former one, which is replaced by a close, nearly the geometric-limit intensity of 6%, peak. The first peak due to its SP origin is expected to be sensitive to n_a. This effect is clearly seen from Fig. 1(b) that displays the spectra computed for three analytes: $n_a = 1.329$ (methanol), 1.333 (water) and 1.359 (ethanol). Fig. 1(c) presents an empirical dependence of the 1st peak position λ_{m1} on n_a. It appears that S_λ (not shown) for the 2nd peak position λ_{m2} is significantly smaller than that for λ_{m1} demonstrating the substrate origin of the 2nd peak. Due to the large sensitivity $S_\lambda \approx 581$ nm/RIU ($DL_\lambda \approx 1.7 \times 10^{-6}$ RIU at $\delta\lambda = 1$ pm) for the 1st peak, it has a great potential for sensing applications, and as a result we continued our investigation of this main peak.

4. Experimental

4.1. Samples

The fabrication of samples involves deposition of a metal layer on a substrate and e-beam lithography for nanostructure patterning, which is one of the physical techniques described e.g. in a very recent review [16]. Ag is deposited on a SiO_2 substrate with the rate of 0.6 Å/s using an electron gun. After the deposition a thin PMMA layer is spin coated and baked at 180 °C for 3 min. The electron beam writing, done by Raith e-line system, uses 20 KeV with low current. A 2 mm long line is written without stitching using Fix Beam Moving Stage (FBMS) mode. After the writing, the PMMA is developed at 22 °C for 45 s using MIBK-IPA (1:3). For etching the Ag lines, PMMA was used as a mask and ion beam milling was done for 4 min. The last fabrication stage includes protecting the etched Ag lines by deposition of a 5-nm thick Au layer, and PMMA encapsulation filling the slits and covering all the

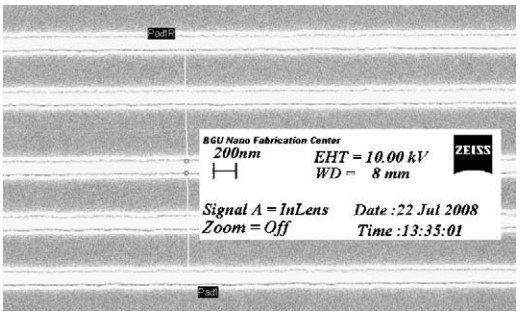

Fig. 2. A SEM image of one of the fabricated nanostructures with specifications as described in the text.

structure by a 20-nm thick layer. A SEM image of one of our samples, the Ag grating with the dimensions $\Lambda = 498.5$ nm, $W = 100$ nm and $H = 45$ nm, fabricated on the SiO_2 substrate and PMMA encapsulated as described above, is shown in Fig. 2.

4.2. Apparatus

To demonstrate sensing, an optical system, shown in Fig. 3, was built. It includes an I/O reflection–transmission setup and a fabricated nanostructure based sensing unit. The input light source is a deuterium–halogen lamp coupled to a 0.6 mm diameter core fiber. The output light at the distal end of the fiber is collimated with a lens, passing through a polarizer and through a pinhole of the same size as the sample and a beam splitter. The transmitted and reflected beams are collected with a lens similar to the collimation lens and are launched into an output fiber connected to a spectrometer. Transmission and reflection signals recorded by the spectrometer were processed using Matlab®. The sample is held on an x–y rotating stage to allow best alignment to the beam and the polarizer. The analytes are dripped and pumped by a digital micropipette.

5. Results and discussion

We measured the spectral responses of our sensor device (Fig. 3), with different fabricated structures as sensing units, to a variety of non-organic liquids, organic and biological analytes. In the cases where all RI are reliably known, we computed the spectra and compared them with the measured ones. To test our measurement system and simulation tool, we started with one of the configurations considered in Section 3—the bare Ag grating contacting the methanol analyte, though at different grating dimensions $\Lambda = 500$ nm, $W = 50$ nm, $H = 45$ nm. For this structure, the measured

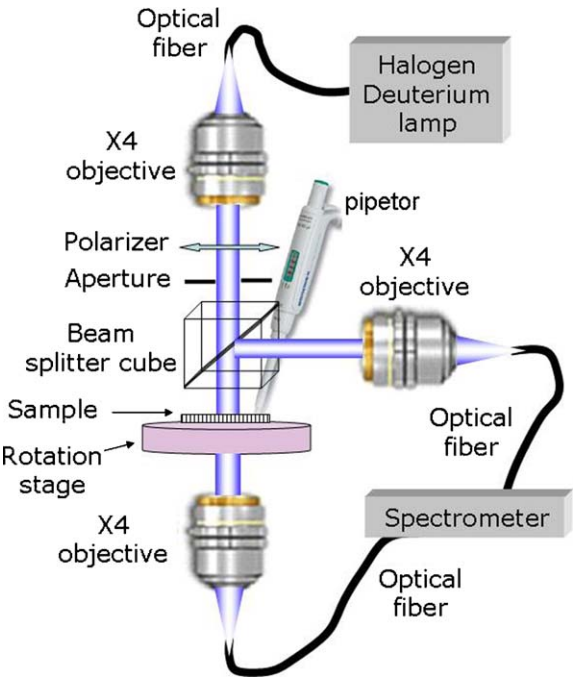

Fig. 3. Experimental setup.

transmission spectrum is shown in Fig. 4 (symbols), which exhibits the two-peak structure theoretically predicted above, see Fig. 1(a and b). Moreover, the simulated normal transmission spectrum (full line), agrees well with the measured one, at least regarding the position and amplitude of the EOT peaks, the agreement is even quantitative around the 2nd peak. Yet, two discrepancies are observed: (i) right to each peak in the measured spectra a small-intensity satellite splits off,

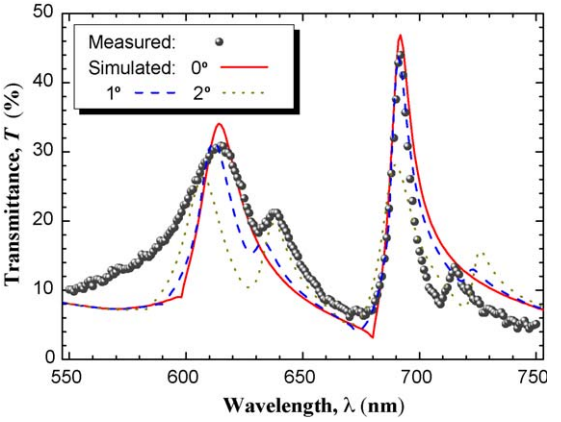

Fig. 4. The transmission spectra of the bare Ag grating with the dimensions $\Lambda = 500$ nm, $W = 50$ nm and $H = 45$ nm, fabricated on the SiO_2 substrate as described in the text, topped by the pure methanol. Ball symbols–measured, lines–simulated for three angles of incidence: 0° (normal), 1° and 2°.

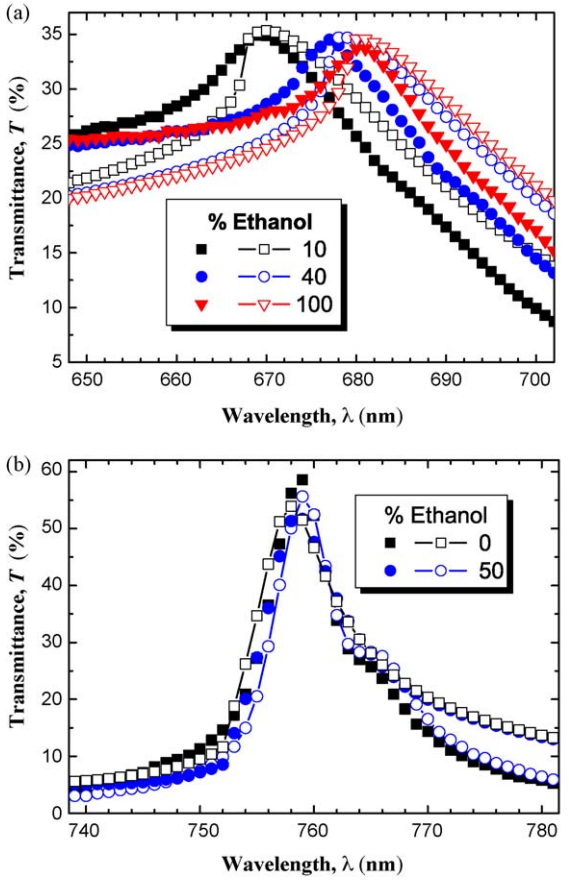

Fig. 5. The transmission spectra of the Ag grating with the dimensions $\Lambda = 498.5$ nm, $W = 100$ nm and $H = 45$ nm, fabricated on the SiO_2 substrate and PMMA encapsulated as described in the text, topped by the DIW–ethanol mixtures. Measured (symbol), simulated (open symbol + lines): (a) zoom around the 1st EOT peak; (b) zoom around the 2nd EOT peak; (c) the 1st EOT peak position vs. the analyte RI, S_λ is determined from the linear regression according to Eq. (1).

which is not found in the simulation; (ii) in the experiment the 1st EOT peak is broader than in the theory. This is likely to be due to incidence offsets, such as an imprecise alignment of the sample surface normally to the beam direction and/or an imperfect collimation, when the incident beam is superposed of a plane waves' continuum with a small but finite propagation fan out. This reasoning is confirmed by the simulations for the incidence angles of 1° (dashed) and 2° (dotted), as shown in Fig. 4. It is seen that in the simulated oblique-incidence spectra, like in the measured one, the satellite peaks do split off the EOT peaks. At the same time, under a unique plane wave incidence at the angles beyond 1°, the 1st EOT peak shifts to the left decreasing in height but it does not broaden (see in Fig. 4). Thus the imperfect collimation would be better explanation of the observation (ii), and we can roughly estimate the polar angle spread as being $\pm 2^\circ$. But this is quite insufficient to account for the above tiny features in detail since it is unknown how to superpose the constituent plane waves in the beam, i.e. what is the degree of coherence and angular spectrum. Eventually, the effects (i)–(ii) are parasitic ones for our sensor, so to get rid of them we improved the optical system.

Fig. 5 shows the transmission spectra measured and computed for the nanostructure, presented by Fig. 2, topped with DIW, pure ethanol, and 10–50% ethanol in DIW solutions. The refractive indices of these analytes are reported in [17]. Only a part of the results is displayed, whereas the conclusions for other ethanol contents are fairly similar. Fig. 5(a) and (b) are zoomed shapes of the spectra near the 1st and 2nd EOT peaks, respectively, where their variation with varying the ethanol percentage is clearly seen. A fair agreement between the theory and experiment around the peaks is observed. Fig. 5(c) shows the extracted experimental and theoretical dependence of λ_{m1} on n_a, which are close to linear. This fact in concurrence with a high (~35%) intensity of the 1st EOT peak may be used for reliable calibration of our device. The experimental sensitivity, estimated from the linear fit shown in Fig. 5(c) is $S_\lambda \approx 439.0$ nm/RIU ($DL_\lambda \approx 2.7 \times 10^{-6}$ RIU), which suits well with the theoretical one $S_\lambda \approx 444.9$ nm/RIU ($DL_\lambda \approx 2.2 \times 10^{-6}$ RIU), see Fig. 5(c).

6. Conclusion

To conclude, by means of numerical case studies of EOT via metallic gratings with narrow slits on a substrate we demonstrated that a short-wavelength EOT peak is highly sensitive to the top ambient (analyte). This is due to attribution of the peak to SP like mode which propagates along the analyte-grating interface. The sensitivity remains high and may even be enhanced by filling the slits and covering the grating using a transparent dielectric, which was PMMA in our study. In addition, we showed that the EOT peaks are highly sensitive to minute incidence angle offsets, which also indicates SP nature of the peaks.

The anticipated regularities were verified experimentally on several few specially fabricated structures, and one of them, the PMMA-protected Ag grating on the silica substrate, showed the best sensitivity ~439–445 nm/RIU, higher than that reported for 2D holes-array grating [6]. Our setup with this sample as sensing unit may be thus viewed as a step towards to prototyping water contamination (e.g. ethanol) sensors.

Acknowledgement

This research is supported by the Israeli Ministry of Science research funding program ''Tashtiot''.

References

[1] D.W. Lubbers, N. Opitz, Die pCO_2/pO_2 optrode: eine neue pCO_2-bzw, pO_2-Messonde zur Messung des pCO_2 oder pO_2 von Gasen und Flussigkeiten, Z. Naturforsch. C 30 (1975) 532–533.

[2] B. Liedberg, C. Nylander, I. Sundstrom, Surface plasmon resonance for gas detection and biosensing, Sens. Actuators 4 (1983) 299–304.

[3] J. Homola, S. Sinclair, G.Y. Gauglitz, Surface plasmon resonance sensors: review, Sens. Actuators B 54 (1999) 3–15.

[4] I. Abdulhalim, M.D. Zourob, A. Lakhtakia, Surface plasmon resonance for bio-sensing: a mini-review, Electromagnetics 28 (2008) 214–242.

[5] T.W. Ebbesen, H.J. Lezec, H.F. Ghaemi, T. Thio, P.A. Wolff, Extraordinary optical transmission through sub-wavelength holes arrays, Nature 391 (1998) 667–669;
H.F. Ghaemi, T. Thio, D.E. Grupp, T.W. Ebbesen, H.J. Lezec, Surface plasmons enhance optical transmission through subwavelength holes, Phys. Rev. B 58 (1998) 6779–6782.

[6] A.G. Brolo, R. Gordon, B. Leathem, K.L. Kavanagh, Surface plasmon sensor based on the enhanced light transmission through arrays of nanoholes in gold films, Langmuir 20 (2004) 4813–4815.

[7] J.A. Porto, F.J. Garcia-Vidal, J.B. Pendry, Transmission resonances on metallic gratings with very narrow slits, Phys. Rev. Lett. 83 (1999) 2845–2848.

[8] I. Avrutsky, Y. Zhao, V. Kochergin, Surface-plasmon-assisted resonant tunneling of light through a periodically corrugated thin metal film, Opt. Lett. 25 (2000) 595–597.

[9] Q. Cao, P. Lalanne, Negative role of surface plasmons in the transmission of metallic gratings with very narrow slits, Phys. Rev. Lett. 88 (2002), 057403-1–4.

[10] P. Lalanne, C. Sauvan, J.P. Hugonin, J.C. Rodier, P. Chavel, Perturbative approach for surface plasmon effects on flat interfaces periodically corrugated by subwavelength apertures, Phys. Rev. B 68 (2003), 125404-1–11.

[11] A. Moreau, C. Lafarge, N. Laurent, K. Edee, G. Granet, Enhanced transmission of slit arrays in an extremely thin metallic film, J. Opt. A: Pure Appl. Opt. 9 (2007) 165–169.

[12] Y. Pang, C. Genet, T.W. Ebbesen, Optical transmission through subwavelength slit apertures in metallic films, Opt. Comm. 280 (2007) 10–15.

[13] K.L. Lee, W.S. Wang, P.K. Wei, Comparisons of surface plasmon sensitivities in periodic gold nanostructures, Plasmonics 3 (2008) 119–125.

[14] M. Auslender, A. Bergel, N. Pinhas, S. Hava, Multi-layered grating diffraction, graphical user interfaced simulation toolbox in the MATLAB environment, Proc. SPIE 5349 (2004) 463–473.

[15] M. Auslender, S. Hava, Scattering-matrix propagation algorithm in full-vectorial optics of multilayer grating structures, Opt. Lett. 21 (1996) 1765–1767.

[16] J.Z. Zhang, C. Noguez, Plasmonic optical properties and applications of metal nanostructures, Plasmonics 3 (2008) 127–150.

[17] R.C. Weast, M.J. Astle, CRC Handbook of Chemistry and Physics, CRC Press, Boca Raton, FL, 1979.